JOURNAL OF THERMOPHYSICS AND HEAT TRANSFER
Vol. 23, No. 2, April–June 2009

# Advanced Model of Silicon Carbide Based Uranium Ceramic Nuclear Fuel Production

Xiaolin Wang*
*Stony Brook University, Stony Brook, New York 11794-2300*
Suraj C. Zunjarrao† and Raman P. Singh†
*Oklahoma State University, Tulsa, Oklahoma 74194*
and
Hui Zhang‡
*Tsinghua University, 100084 Beijing, People's Republic of China*

DOI: 10.2514/1.38865

**A system-level model combining heat and mass transport and chemical reaction is developed to study silicon-carbide-based uranium ceramic material processing. This process is based on pyrolysis and synthesis of a mixture of preceramic polymers and uranium oxide particles. Three key steps for polymer pyrolysis and one key reaction for uranium oxide and silicon carbide interaction are established for the processing. The mechanism of vapor species transport is described by introducing a driving force induced by both natural and forced convection. The effects of geometry of sample, driving force, and particle size and volume fraction of filler, uranium oxide, on the porosity evolution, species uniformity, and reaction rate of the sample are investigated.**

## Nomenclature

| | | |
|---|---|---|
| $C_p$ | = | specific heat at constant pressure, J/kg · K |
| $d_p$ | = | equivalent average particle diameter, m |
| $d$ | = | particle diameter, m |
| $E_a$ | = | activation energy, J/mol |
| $f$ | = | volume fraction |
| $K$ | = | permeability, $m^2$ |
| $k$ | = | thermal conductivity, W/m · K |
| $M$ | = | mass, kg |
| $n$ | = | ratio of diameter of large particles and small particles |
| $P$ | = | pressure, Pa |
| $q''$ | = | heat flux, $W/m^2$ |
| $R$ | = | reaction rate |
| $R$ | = | universal gas constant, 8.314 J/mol · K |
| $r$ | = | radial coordinate |
| $T$ | = | temperature, K |
| $T(\varepsilon)$ | = | tortuosity |
| $t$ | = | time, s |
| $u$ | = | velocity vector |
| $u_r$ | = | radial velocity, m/s |
| $u_z$ | = | axial velocity, m/s |
| $V$ | = | volume, $m^3$ |
| $Y$ | = | species mass fraction |
| $Z$ | = | preexponential |
| $\Delta H$ | = | heat of reaction, J/mol |
| $\Delta P_1$ | = | driving force induced by natural convection, Pa |
| $\Delta P_2$ | = | driving force induced by forced convection, Pa |
| $\Delta Z$ | = | elevation difference, m |
| $\varepsilon_m$ | = | emissivity |
| $\varepsilon$ | = | porosity |
| $\mu$ | = | viscosity, kg/m · s |
| $\rho$ | = | density, $kg/m^3$ |

*Subscripts*

| | | |
|---|---|---|
| eff | = | effective |
| $g$ | = | gas |
| $r$ | = | radial direction |
| $s$ | = | mixed solid |
| side | = | side surface |
| top | = | top surface |
| total | = | total |
| $\infty$ | = | surrounding |
| 0 | = | reference |
| 1 | = | first reaction, uranium oxide |
| 2 | = | second reaction, polymer |
| 3 | = | third reaction |

## I. Introduction

AMONG the various advanced ceramics, silicon carbide (SiC) displays a number of superior characteristics as a structural material, such as its thermal and mechanical properties, chemical stability, and low radioactivation. Moreover, irradiation effects on swelling and mechanical properties of high-purity SiC have been evaluated, and excellent high-temperature irradiation resistance has been reported by several researchers [1,2]. SiC matrix composites have been widely developed for use in advanced energy systems [3–5]. These properties make SiC a promising candidate for use in nuclear applications as inert-matrix material. In addition, uranium carbide (UC) is an attractive fuel for certain generation IV reactors, such as the gas-cooled fast reactor, due to its high thermal conductivity and high melting point. Therefore, ceramic composite pellets consisting of UC particles in a SiC matrix can be used as high-temperature refractory ceramic fuels due to excellent characteristics of both UC and SiC.

SiC-based uranium ceramic materials can be obtained through reaction of a preceramic polymer and $U_3O_8$ particles. The processing cycle involves curing of a polymer precursor at 150–250°C, in which the polymer undergoes crosslinking to form a green body, followed by a pyrolysis stage that involves the formation of amorphous SiC at 400–900°C and crystallization of SiC and formation of UC at 1000–1500°C. This technique allows for the fabrication of SiC-based uranium ceramic materials at a lower temperature compared to a sintering technique. In addition, it offers fabricating net-shape components without suffering from maximum components size limitations such as that of chemical vapor deposition or ultrasonic

Received 31 May 2008; revision received 9 December 2008; accepted for publication 11 December 2008. 

*Department of Mechanical Engineering.
†School of Mechanical and Aerospace Engineering.
‡Department of Engineering Physics.

machining [6]. Moreover, it provides better geometrical accuracy compared to conventional ceramics at significantly lower manufacturing temperatures [7,8] and offers flexibility of fabricating refractory ceramic composites and novel mixed-metal carbide systems with controlled microstructure (at submicron and nano levels), graded and fiber reinforced configurations, and a wide range of compositional control.

It has been found that, for the pyrolysis of polymer mixed with filler particles, particle size and volume fraction of the filler significantly influence the porosity evolution and reaction rate [4,9]. In addition, the operating conditions, such as the heating rate and operating pressure, strongly affect the material property and long-term stability. Because of the long duration of the fabrication process and the difficulties in the in situ measurements, it is important to build a system-level model for process simulation and key control parameters identification. The model should be capable of describing heat and mass transfer, chemical reaction, and porosity evolution of $U_3O_8$ mixed polymer. A series of concurrent and consecutive chemical reactions are involved in $U_3O_8$ mixed polymer pyrolysis and synthesis. However, the nature and extent of these reactions are not sufficiently defined. Therefore, it is useful to consider key reactions and controlling parameters to understand the fabrication process [10].

Numerical simulations have been widely used to study pyrolysis kinetics of different materials, such as source material decomposition in sublimation system [11], cigarette smoldering [12], biomass pyrolysis [13], and food pyrolysis [14]. In these applications, all materials are treated as porous media. However, only limited literature is available for metal mixed polymer pyrolysis and synthesis, mostly experimental efforts. Staggs presented a thermal degradation model for polymer pyrolysis using one-step first-order kinetics [10]. The model solves single component polymer pyrolysis. However, polymer pyrolysis is usually a multistep reaction, resulting in a set of kinetic equations.

The goal of this work is to develop an integrated model to predict pyrolysis and synthesis of $U_3O_8$ mixed polymer. It needs to consider polymer pyrolysis and interaction between two different components. Three key reactions for polymer pyrolysis and one key reaction between $U_3O_8$ and SiC are presented. The mechanism of vapor species transport and a set of conservation equations for the entire process are developed. Effects of transport processes such as heat up, polymer decomposition, and vapor species transport are included. Pyrolysis and sintering of a sample with different geometries are simulated to study the effects of the sample geometry on the uniformity of the final product. In addition, effects of driving force, particle size, and volume fraction of filler on the porosity evolution and reaction rate are studied.

## II. Experiments and Results

Allylhydridopolycarbosilane (AHPCS), acquired from Starfire Systems, Inc., Malta, New York (SMP-10), is an olefin-modified polymer that undergoes pyrolysis when heated under inert atmosphere and yields near stoichiometric SiC. Carefully weighed quantities of liquid AHPCS were heated, under argon atmosphere, from room temperature up to 300, 500, 700, and 900°C, respectively, to establish the kinetics of the AHPCS pyrolysis. Samples were held at final temperatures for 30 min to ensure thermal equilibrium. Upon heating, the polymer precursor yields a dry and partially crosslinked solid, for example, a green body, at 300°C; this step is called curing. A box furnace was fitted with a retort and modified for the inert gas pyrolysis up to 900°C, and pyrolysis beyond 900°C was performed in a specially modified high-temperature furnace (model no. F46248, Barnstead International, Dubuque, Iowa). In addition, small quantities of amorphous SiC derived from AHPCS pyrolyzed at 900°C were heated to different temperatures of 1150, 1400, and 1650°C under a constant flow of argon.

Figure 1 shows the ceramic yield as a function of decomposition temperature. The experimental data were measured immediately after the temperature of the samples reached certain temperatures (300, 500, 700, 900, and 1150°C). The loss in weight is attributed to

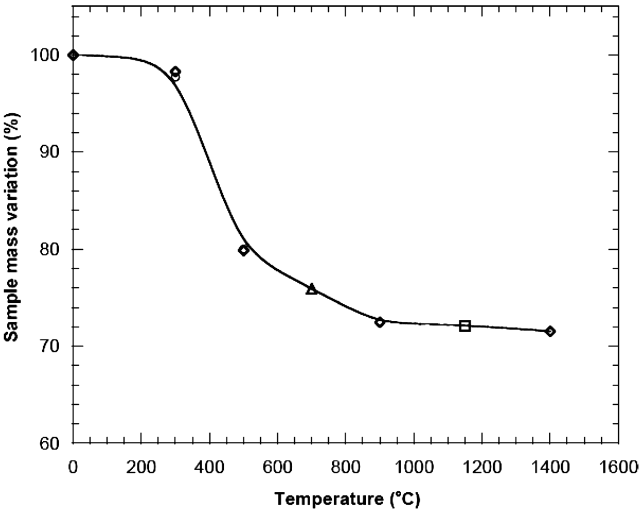


**Fig. 1 Mass loss variation as a function of temperature for AHPCS.**

the loss of low-molecular weight oligomers and hydrogen gas [15]. About 72–74% ceramic yield in the form of amorphous SiC was obtained in the range of 900–1650°C. The material processed to 1150°C is stoichiometric SiC, as discussed in [16].

Fourier transform infrared (IR) spectroscopy analysis was performed to study the polymer-ceramic conversion. Figure 2 shows the IR spectra obtained for the products at temperatures of 300, 500, 700, 900, and 1150°C. Peaks attributed to C-H (stretching), Si-H (stretching), and Si-C (rocking) bonds were clearly observed in the range of 2800–3000 $cm^{-1}$, 2000–2140 $cm^{-1}$, and 870–1070 $cm^{-1}$, respectively [15,17,18]. It can be seen that relative intensity of all the peaks initially increases with increasing temperature, which is a result of increase in crosslink density as the polymer cures, forming a network structure. A gradual shift in the Si-H peak toward higher frequencies, with increasing temperatures, suggests conversion of silicon–hydrogen bonding from $Si-H_3$ to $Si-H_2$ to Si-H, as hydrogen is released. The broad peak attributed to several C-H bonds reduces, and eventually disappears, along with the Si-H peak at 1150°C as hydrogen is completely removed. Small peaks resulting from the presence of monosubstituted alkenes in the polymer appear around 900 $cm^{-1}$ (d on the figure) at 300°C and 500°C and soon disappear at higher temperatures. Peaks attributed to $CH_3$ (bending) (a and b on the figure) and $SiCH_2Si$ bonding (c on the figure) are also identified in the IR spectra. A small amount of hydrogen appears to be present in the system even at 900°C, whereas at 1150°C only a SiC peak shows complete conversion of polymer into SiC.

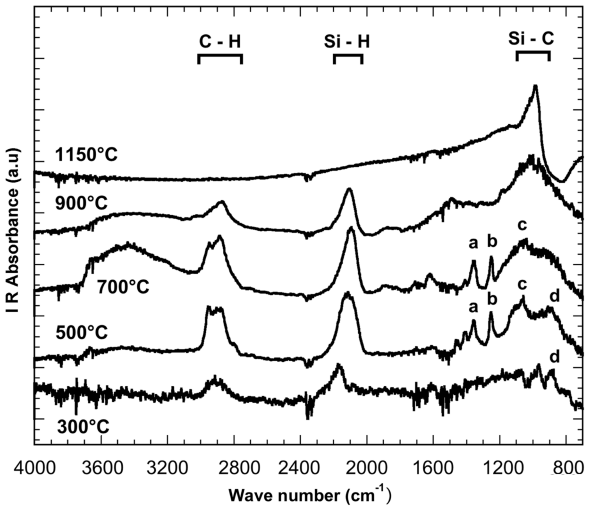


**Fig. 2 Infrared spectra for AHPCS heated to 300, 500, 700, 900, and 1150°C.**

A ceramic composite consisting of an amorphous silicon carbide (a-SiC) matrix that contained $U_3O_8$ particles (International Bio-Analytical Industries, Boca Raton, Florida) was fabricated using AHPCS. The resulting sample had a good dispersion of uranium oxide particles in an a-SiC matrix. However, it contains numerous pores as a result of the release of hydrogen and other vapor species during the polymer pyrolysis.

The reaction kinetics of SiC and $U_3O_8$ particles are yet to be established. Nevertheless, this paper provides the framework to model the fabrication process. Once this chemistry is established experimentally, the relevant parameters will serve as input into the process model presented.

## III. Reaction Kinetics

Polymer pyrolysis process is characterized by three key steps. The first step is volatilization (polymer, denoted as $A \rightarrow$ intermediate product, denoted as $B$) and occurs at 300–500°C, in which $H_2$ is generated and released. The second step is the crosslink process (intermediate product, $B \rightarrow$ amorphous SiC, denoted as $C$) at 500–900°C, in which amorphous SiC is formed. The third step is crystallization of SiC (amorphous SiC, $C \rightarrow$ crystallized SiC, denoted as $D$) and occurs when temperature is above 1000°C. It should be noted that curing of the polymer precursor is not considered in our model. $A$, $B$, $C$, and $D$ are all in the solid phase.

These three key reactions are incorporated into the polymer pyrolysis model, as well as a single reaction for the interaction between SiC and $U_3O_8$. The reactions are expressed as follows:

$$1\ \text{kg}\,A \rightarrow \alpha_1\,\text{kg}\,B + (1-\alpha_1)\text{kg}\,P_1 \tag{1}$$

$$1\ \text{kg}\,B \rightarrow \alpha_2\,\text{kg}\,C + (1-\alpha_2)\text{kg}\,P_2 \tag{2}$$

$$1\ \text{kg}\,C \rightarrow 1\ \text{kg}\,D \tag{3}$$

$$1\ \text{kg SiC} + \alpha_3\,\text{kg}\,U_3O_8 \rightarrow \alpha_4\,\text{kg UC} + \alpha_5\,\text{kg products} + (1+\alpha_3-\alpha_4-\alpha_5)\text{kg}\,P_3 \tag{4}$$

where $P_1$, $P_2$, and $P_3$ represent vapor species produced. It should be noted that reaction (3) is a phase transformation process (amorphous SiC $\rightarrow$ crystallized SiC), and $U_3O_8$ remains chemically unchanged when the temperature is below 1200°C. In addition, the reaction between SiC and $U_3O_8$ is not known yet, but UC is assumed to be produced.

The first-order reaction kinetics is assumed for simplicity in this work, and the parameters are obtained by fitting the experimental data (see Sec. V). The rates of the preceding reactions are given by the Arrhenius relation [19]:

$$\dot{R}_1 = (1-\varepsilon)\rho_s Y_A Z_1 \exp(-E_1/RT) \tag{5}$$

$$\dot{R}_2 = (1-\varepsilon)\rho_s Y_B Z_2 \exp(-E_2/RT) \tag{6}$$

$$\dot{R}_3 = (1-\varepsilon)\rho_s Y_C Z_3 \exp(-E_3/RT) \tag{7}$$

$$\dot{R}_4 = (1-\varepsilon)\rho_s Y_{\text{SiC}}(1-\varepsilon)\rho_s Y_{U_3O_8} Z_4 \exp(-E_4/RT) \tag{8}$$

where $Y_i$ with $i = A, B, C$ is the mass fraction of species $i$ in the mixture, that is, $Y_i = M_i/M_s$, where $M_i$ is the mass of species $i$ in the mixture, and $M_s$ is the mass of the mixed solid. $Z_j$ with $j = 1, 2, 3, 4$ is the preexponential of the $j$th reaction rate, $E_j$ is the activation energy of the $j$th reaction, and $R$ is the universal gas constant. The mass change rates of $A$, $B$, $C$, and $D$ and the mixed solid are defined by

$$\dot{M}_A = -\dot{R}_1 \tag{9}$$

$$\dot{M}_B = \alpha_1\dot{R}_1 - \dot{R}_2 \tag{10}$$

$$\dot{M}_C = \alpha_2\dot{R}_2 - \dot{R}_3 \tag{11}$$

$$\dot{M}_D = \dot{R}_3 \tag{12}$$

$$\dot{M}_s = -(1-\alpha_1)\dot{R}_1 - (1-\alpha_2)\dot{R}_2 - (1+\alpha_3-\alpha_4-\alpha_5)\dot{R}_4 \tag{13}$$

The three terms on the right-hand side of Eq. (13) are the mass production rates of vapor species $P_1$, $P_2$, and $P_3$, respectively.

## IV. Mathematical Models

The following assumptions are made in developing the computational equations:

1) The vapor species flow is transient and laminar.

2) The vapor species and solid phases are at the same temperature locally.

3) The densities of two different particles (polymer and $U_3O_8$) remain constant during decomposition.

### A. Mass Conservation for Source Components

Figure 3 shows the schematic of the model. The crucible is a cylinder. The computational domain consists of gases, the filler particles, and the polymer matrix. This domain is considered a porous medium. The yield of both components, for example, the polymer and the filler, is a key issue in the model. Therefore, for numerical convenience, it is desirable to introduce the void fractions for both components. We define $\varepsilon_1$ as the specific void fraction of $U_3O_8$ and its yield in the total volume of the mixture, and $\varepsilon_2$ as the specific void fraction of polymer and its yield in the remaining void volume of the mixture:

$$\varepsilon_1 = \frac{V_{\text{total}} - V_1}{V_{\text{total}}} \tag{14}$$

$$\varepsilon_2 = \frac{V_{\text{total}} - V_1 - V_2}{V_{\text{total}} - V_1} \tag{15}$$

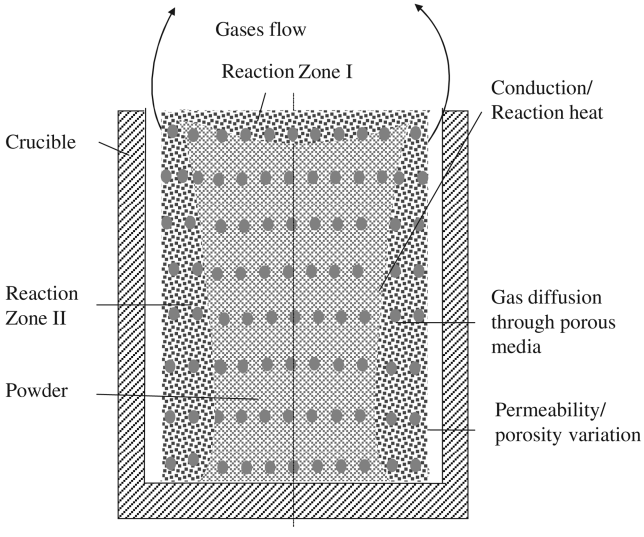


**Fig. 3 Schematic of the computational domain in the process model.**

where $V_1$, $V_2$, and $V_{\text{total}}$ are volumes of $U_3O_8$, polymer, and total volume. Thus, the porosity of the porous medium $\varepsilon$ is defined as

$$\varepsilon = \varepsilon_1 \times \varepsilon_2 = \frac{V_{\text{total}} - V_1 - V_2}{V_{\text{total}}} \tag{16}$$

The volume fractions of $U_3O_8$ and polymer, $f_1$ and $f_2$, can be calculated as

$$f_1 = \frac{V_1}{V_1 + V_2} = \frac{1 - \varepsilon_1}{1 - \varepsilon} \tag{17}$$

$$f_2 = 1 - f_1 \tag{18}$$

The density of the mixed solid is expressed as follows:

$$\rho_s = \rho_1 f_1 + \rho_2 f_2 \tag{19}$$

where $\rho_1$ and $\rho_2$ are densities of $U_3O_8$ and polymer, respectively. Based on the preceding assumptions and definitions, the conservation of $U_3O_8$ and polymer is given by

$$\frac{\partial[\rho_1 f_1(1-\varepsilon)]}{\partial t} = (\alpha_4 - \alpha_3)\dot{R}_4 \tag{20}$$

$$\frac{\partial[\rho_2 f_2(1-\varepsilon)]}{\partial t} = -(1-\alpha_1)\dot{R}_1 - (1-\alpha_2)\dot{R}_2 - (\alpha_4 - \alpha_3)\dot{R}_4 \tag{21}$$

Yields of both components can be obtained based on Eqs. (20) and (21).

### B. Mass Conservation for Mixed Vapor Species

The equation of continuity in the cylindrical coordinate is ([20], p. 276)

$$\frac{\partial}{\partial t}[\rho_s(1-\varepsilon) + \rho_g \varepsilon] + \frac{1}{r}\frac{\partial}{\partial r}(r\varepsilon\rho_g u_r) + \frac{\partial}{\partial z}(\varepsilon\rho_g u_z) = 0 \tag{22}$$

where $\rho_g$ is the mass density of vapor species, and $u_r$ and $u_z$ are the velocity component of vapor species in the radial and axial directions, respectively.

It is assumed that the diffusive transport of vapor species is comparatively smaller than the convective transport; therefore, the diffusion in the gas mixture phase is neglected. Gas pressure in the porous medium can be derived from the Darcy's law:

$$\nabla P = -\frac{\mu}{K}\mathbf{u} \tag{23}$$

where $K$ is the local permeability of the porous medium. To calculate the permeability, we assume that the polymer matrix is composed of very compacted microparticles (10 $\mu$m in diameter). The permeability of the porous media is assumed to be

$$K(\varepsilon) = \frac{[d_p(f_1)]^2 \varepsilon^3}{36K_0(1-\varepsilon)^2[T(\varepsilon)]^2} \tag{24}$$

where $d_p(f_1)$ and $T(\varepsilon)$ are the equivalent average particle diameter and tortuosity, respectively [19]. The details of $d_p(f_1)$ and $T(\varepsilon)$ can be found in [19].

Reaction starts from both side and top surfaces of the porous medium, and two reaction zones (reaction zones I and II in Fig. 3) are formed. It is assumed that vapor species produced in reaction zone I escape from the top surface of the porous medium with $u_z$ only, and $u_r$ is negligible in Eq. (22). Therefore, in reaction zone I, the momentum equation can be simplified as

$$P(r,z) = P_{\text{top}}(r) + \int_z^H \frac{\mu}{K(r,z)} u_z(r,z)\,\mathrm{d}z \tag{25}$$

where $H$ is the height of the porous medium, and $P_{\text{top}}(r)$ is the gas pressure at the top surface of the porous medium. We define $\Delta P(r,z)$ as the pressure difference between the location $(r,z)$ and the top surface

$$\Delta P(r,z) = P(r,z) - P_{\text{top}}(r) \tag{26}$$

Similarly, vapor species produced in reaction zone II escape from the side surface of the porous medium with $u_r$ only. In reaction zone II, the momentum equation can be simplified as

$$P(r,z) = P_{\text{side}}(z) + \int_r^R \frac{\mu}{K(r,z)} u_r(r,z)\,\mathrm{d}r \tag{27}$$

where $R$ is the height of the porous medium, $P_{\text{side}}(z)$ is the gas pressure at the side surface of the porous medium, and $\Delta P(r,z)$ is the pressure difference between the location $(r,z)$ and the side surface:

$$\Delta P(r,z) = P(r,z) - P_{\text{side}}(z) \tag{28}$$

Polymer pyrolysis is related to both porous medium temperature and vapor species transport. Vapor species can escape from the porous medium by the driving force induced by both natural and forced convection.

The driving force, designated by $P_{\text{df}}$, is a product of both natural and forced convection. The forced convection leads to the pressure difference $\Delta P_f$ between the furnace and outside environment; it can be adjusted in experiments. If the furnace is open, then $\Delta P_f = 0$. The driving force induced by natural convection $\Delta P_n$ is due to the density difference between vapor species at the top or side surface of the porous medium and that at the environment. $\Delta P_n$ can be expressed as a function of temperature difference. It should be noted that there exists the buoyant force due to the density difference between vapor species and air even if the temperature is the same. For simplicity, it has been neglected. Therefore,

$$P_{\text{df}} = \Delta P_f + \Delta P_n \tag{29}$$

$$\Delta P_n = \rho_{\text{argon}} g \beta \Delta T \Delta Z \tag{30}$$

where $\beta$ is the thermal expansion coefficient for the argon gas, $\Delta Z$ is the elevation difference, and $\Delta T$ in reaction zones I and II are expressed as follows:

$$\Delta T = T(r,H) - T_\infty \tag{31}$$

$$\Delta T = T(R,z) - T_\infty \tag{32}$$

This model assumes that the vapor species can escape from the porous medium only when the driving force is greater than $\Delta P(r,z)$, the pressure barrier for the vapor species to escape from the porous medium. Because the pressure increases from the outer surface toward the center of the porous medium, polymer near the side and top of the porous medium decomposes first. Reaction zones I and II, therefore, propagate from the outer surface of the porous medium to the center (see Fig. 3).

### C. Energy Conservation Equation

The heat transfer model determines the temperature distribution that serves as input to the kinetics model. The conservation of energy is expressed as [8,21,22]

$$(\rho c_p)_{\text{eff}}\left[\frac{\partial T}{\partial t} + \frac{1}{r}\frac{\partial(uT)}{\partial r}\right] = \frac{\partial}{\partial x}\left(k_{\text{eff}}\frac{\partial T}{\partial x}\right) + \frac{1}{r}\frac{\partial}{\partial r}\left(r k_{\text{eff}}\frac{\partial T}{\partial r}\right) + \sum_{i=1}^{4}\Delta H_i R_i \tag{33}$$

where $k_{\text{eff}}$ is the effective thermal conductivity, and $\Delta H_i$ is the $i$th reaction heat. It should be noted that, in the experiments, the reaction heat is provided from the furnace, that is, from the external source.

The reaction heats do not seem high. In addition, the reaction heats cannot be obtained experimentally or analytically. Therefore, the reaction heats are assumed as zero in the computation. In addition, $(\rho c_p)_{\text{eff}}$ is the effective heat capacity, which can be expressed as

$$(\rho c_p)_{\text{eff}} = (1-\varepsilon)(\rho c_p)_s + \varepsilon(\rho c_{pg}) \tag{34}$$

where $(\rho c_p)_s$ consists of two components

$$(\rho c_p)_s = (\rho c_p)_{s,1} f_1 + (\rho c_p)_{s,2} f_2 \tag{35}$$

where $(\rho c_p)_{s,1}$ and $(\rho c_p)_{s,2}$ are the heat capacities of $U_3O_8$ and polymer, respectively, and $f_1$ and $f_2$ are the volume fractions of $U_3O_8$ and polymer, respectively.

Radiation heat transfer in the porous medium can be incorporated into the effective thermal conductivity. The effective thermal conductivity $k_{\text{eff}}$ can be estimated as [22]

$$k_{\text{eff}} = \varepsilon\left(k_g + \frac{32}{3}\varepsilon_e \sigma T^3 d_p\right) + (1-\varepsilon)k_s \tag{36}$$

where $k_g$ and $k_s$ are effective thermal conductivities of gases and solids in the porous medium, respectively. Emissivity is $\varepsilon_e$, $\sigma = 5.67 \times 10^{-8}$ W/m$^2 \cdot$ K$^4$ is the Stefan–Boltzmann constant, and $d_p$ is the equivalent average pore diameter. The thermal conductivity can be taken as the volume-weighted average, formulated as

$$k_s = f_1 k_{s,1} + f_2 k_{s,2} \tag{37}$$

where $k_{s,1}$ and $k_{s,2}$ are effective thermal conductivities of $U_3O_8$ and polymer, respectively.

The model equations are solved using the finite difference method [11,23]. The computational code is modified from an original code for simulating cigarette smoldering process [12]. The original code is capable of simulating the pyrolysis (one-step reaction) of a single component, such as evolution of porosity and yield of a single component [12]. Our code can simulate several reactions for multicomponents, such as evolution of porosity and yield of all the components. Moreover, the driving force for volatiles escape and the developed mechanism of volatiles escape is included in the code. The solution strategy can be expressed as in the following scheme:

1) Assume the initial state distribution includes the porosities, temperature, and velocity.

2) According to reaction kinetics equations, calculate reaction rates.

3) Calculate velocity component of vapor species $u_r$ and $u_z$.

4) Calculate pressure $P(r, z)$ and driving force $P_{\text{df}}$. Determine the volatiles transport, and calculate porosities, mass and mass fractions of all the solid species.

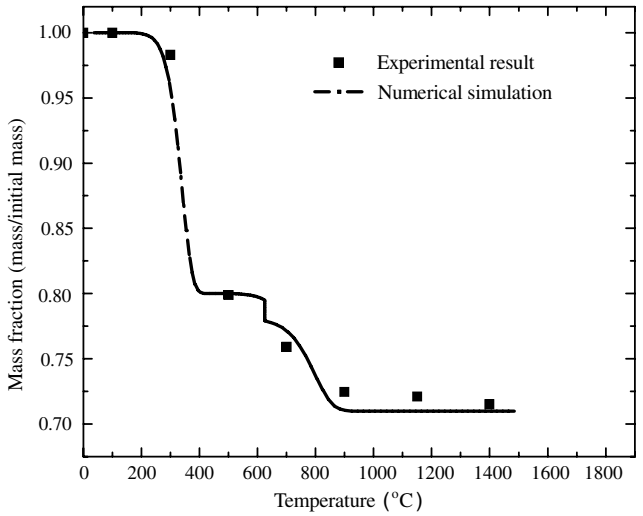


**Fig. 4 Comparison of numerical and experimental mass variation as a function of processing temperature for AHPCS.**

**Table 1 Thermophysical properties used in the calculations**

| Parameter | Value used in program |
|---|---|
| $c_{pg}$, J/kg · K | 1600 |
| $c_{ps,1}$, J/kg · K | 1080 |
| $c_{ps,2}$, J/kg · K | 1080 |
| $k_{s,1}$, W/m · K | 100 |
| $k_{s,2}$, W/m · K | 100 |
| $k_g$, W/m · K | 0.1859 |
| $\rho_{s,1}$, kg/m$^3$ | 8600 |
| $\rho_{s,2}$, kg/m$^3$ | 2500 |
| $\rho_g$, kg/m$^3$ | 0.15 |
| $\mu$, kg/m s | $2.149 \times 10^{-5}$ |
| $E_3/R$, K | $2 \times 10^4$ |
| $\varepsilon_e$ | 0.8 |

5) Find new temperature distribution according to the energy balance on the new time-step explicitly.

6) Repeat steps 2–5.

## V. Results and Discussion

The preexponential constants $Z_1$ and $Z_2$ and the activation energies $E_1$ and $E_2$ are obtained by modeling the pyrolysis of a small polymer sample using the lump analysis. Simulation is performed assuming thermal equilibrium condition. The sample was held at given temperatures for 30 min to ensure thermal equilibrium in the experiments (see Sec. II). Figure 4 shows the comparison of numerical and experimental mass variation (see Fig. 1) as a function of temperature. $Z_1$ and $Z_2$ are calculated to be $1 \times 10^4$ and $2 \times 10^4$, respectively. $E_1$ and $E_2$ are calculated to be $8.3 \times 10^4$ J/mol and $1.5 \times 10^5$ J/mol, respectively.

Basic thermal and physical properties used in the simulation are listed in Table 1. Constant heat flux $q''$ is applied to the boundaries. The polymer yield is defined as the mass ratio between the remaining polymer and initial polymer. Moreover, the polymer matrix is assumed to be compacted microparticles ($d_2 = 10$ $\mu$m). It is noted that the results shown in this paper consider only polymer pyrolysis. $U_3O_8$ is assumed to be passive due to the unknown kinetics of the reaction between SiC and $U_3O_8$. Furthermore, $U_3O_8$ remains unchanged when the temperature is below 1200°C.

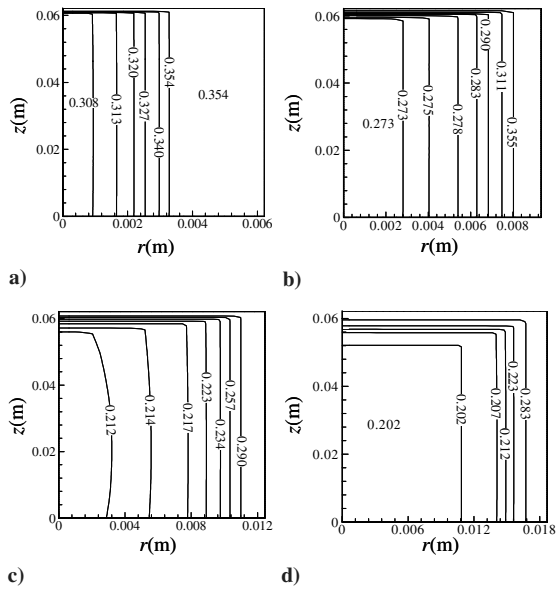


**Fig. 5 Comparison of porosity distributions for different sample size after 40 h reaction. Heat flux $q'' = 0.9$ W/m$^2$, $d_1 = 200$ $\mu$m, and initial porosities are $\varepsilon = 0.2$ and $\varepsilon_2 = 0.3$, respectively: a) sample radius = 6.2 mm, b) sample radius = 9.3 mm, c) sample radius = 12.4 mm, and d) sample radius = 18.6 mm.**

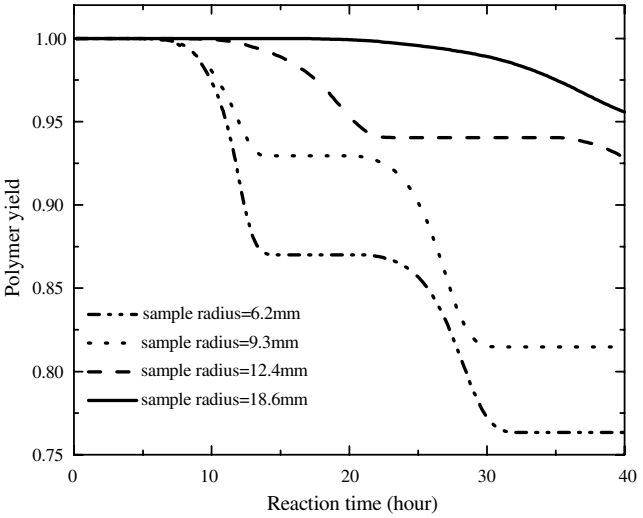


**Fig. 6 Comparison of polymer yields for different sample size. Heat flux $q'' = 0.9$ W/m$^2$, $d_1 = 200$ $\mu$m, and initial porosities are $\varepsilon = 0.2$ and $\varepsilon_2 = 0.3$, respectively.**

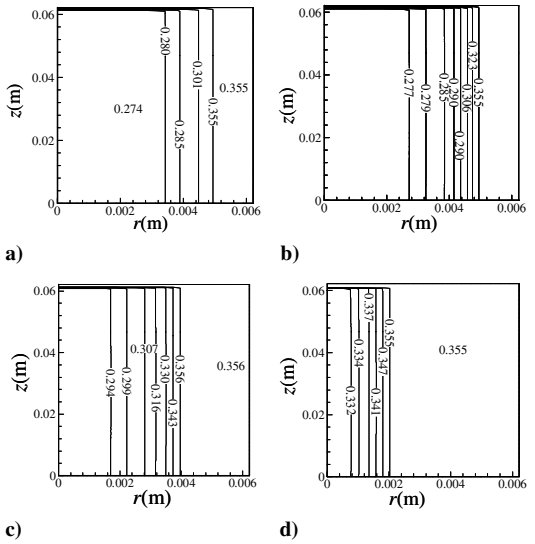


**Fig. 7 Comparison of porosity distributions for different driving force after 40 h reaction. Heat flux $q'' = 0.9$ W/m$^2$, $d_1 = 40$ $\mu$m, and initial porosities are $\varepsilon = 0.2$ and $\varepsilon_2 = 0.3$, respectively: a) $\Delta P_1 = 0$, b) $\Delta P_1 = 500$ Pa, c) $\Delta P_1 = 1000$ Pa, and d) $\Delta P_1 = 1500$ Pa.**

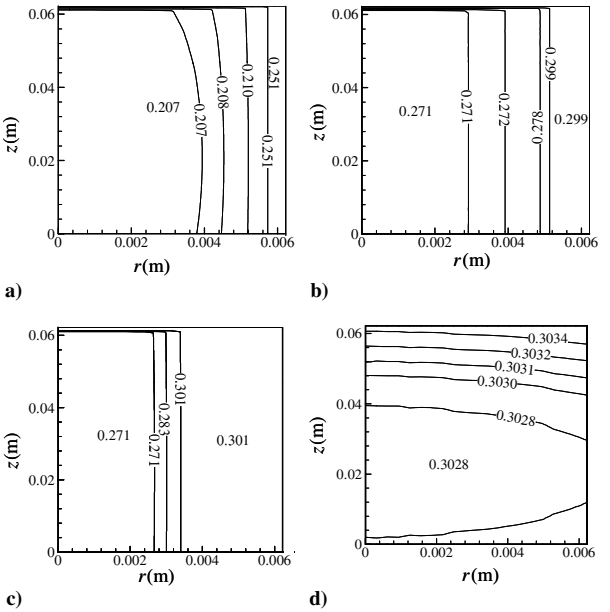


**Fig. 9 Comparison of porosity distributions for different uranium oxide diameters $d_1$ after 25 h reaction. Heat flux $q'' = 0.9$ W/m$^2$, and initial porosities are $\varepsilon = 0.2$ and $\varepsilon_2 = 0.3$, respectively: a) $d_1 = 40$ $\mu$m, b) $d_1 = 100$ $\mu$m, c) $d_1 = 200$ $\mu$m, and d) $d_1 = 400$ $\mu$m.**

The transport phenomena are studied. First, the effect of sample geometry on the uniformity of product and the reaction rate is presented. The radius of the sample is 6.2, 9.3, 12.4, and 18.6 mm, respectively. The height of the sample is 62 mm for all the cases. The heat flux is $q'' = 0.9$ W/m$^2$, reaction time is 40 h, diameter of the filler is $d_1 = 100$ $\mu$m, and initial porosities are $\varepsilon = 0.2$ and $\varepsilon_2 = 0.3$, respectively. Figures 5 and 6 show the comparison of the porosity distribution and polymer yield. It is shown that polymer pyrolysis starts from the side and top surfaces of the porous medium. The porosity gradient, which can reflect the uniformity of the product, is higher for the sample with a larger radius, indicating that the product uniformity is lower. Moreover, the reaction zone and rate decrease as the sample radius increases, because the pressure barrier $\Delta P(r, z)$ increases as the sample radius increases, making it more difficult for the vapor species to escape. At a certain temperature range (reaction time around 15–25 h), a plateau is formed because reactions at lower temperatures are completed and reactions at higher temperatures are very slow. In the experimental data, a linear temperature distribution is observed, as shown in Fig. 4. This is due to many concurrent and

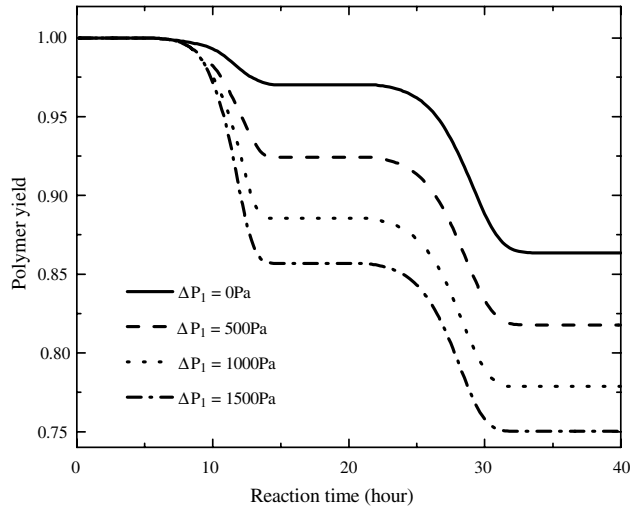


**Fig. 8 Comparison of polymer yields for different driving force. Heat flux $q'' = 0.9$ W/m$^2$, $d_1 = 40$ $\mu$m, and initial porosities are $\varepsilon = 0.2$ and $\varepsilon_2 = 0.3$, respectively.**

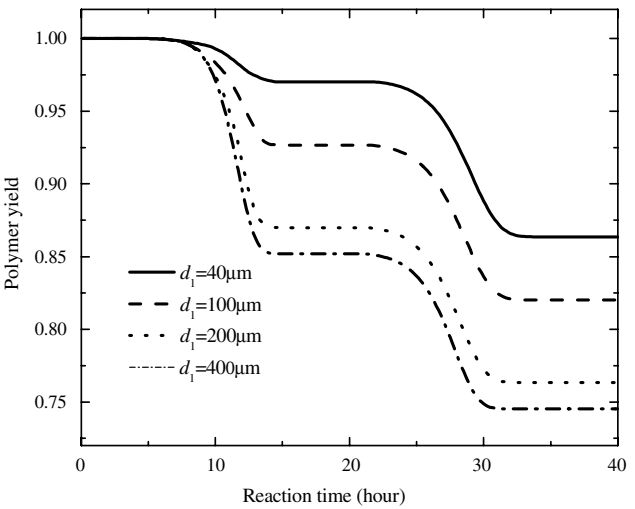


**Fig. 10 Comparison of polymer yields for different uranium oxide diameters $d_1$. Heat flux $q'' = 0.9$ W/m$^2$, and initial porosities are $\varepsilon = 0.2$ and $\varepsilon_2 = 0.3$, respectively.**

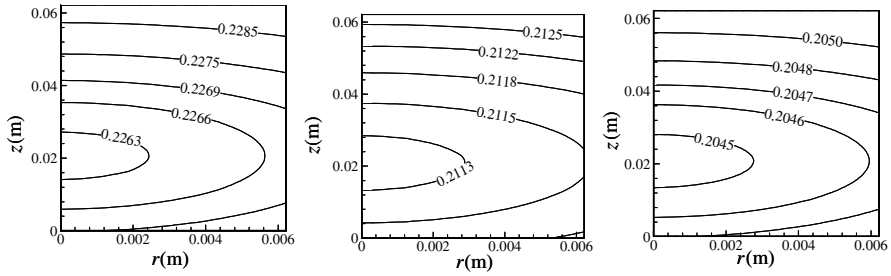


a) $V_1$=0.5$V_2$ b) $V_1$=$V_2$ c) $V_1$=2$V_2$

**Fig. 11 Comparison of porosity distributions for different volume ratios $V_1/V_2$ after 10 h reaction. Heat flux $q'' = 0.9$ W/m$^2$, $d_1 = 100$ $\mu$m, and initial porosity $e = 0.2$.**

consecutive reaction steps involved in the experiments. Nevertheless, because only four reactions and simplified reaction kinetics are considered in our simulation, a plateau is expected.

Second, the effect of driving force from forced convection $\Delta P_f$ on the growth rate is investigated. It plays an important role in the reaction rate because it helps vapor species to escape, leading to the increase of the reaction zone size and reaction rate. Figure 7 shows a comparison of porosity distribution for $\Delta P_f = 0$, 500, 1000, and 1500 Pa. The heat flux is $q'' = 0.9$ W/m$^2$, reaction time is 40 h, diameter of filler particles is $d_1 = 40$ $\mu$m, and initial porosities are $\varepsilon = 0.2$ and $\varepsilon_2 = 0.3$, respectively. It can be concluded that reaction zone size is increased by increasing the forced convection. Also, the porosity gradient decreases as $\Delta P_f$ increases, which indicates the uniformity of the product is enhanced. Figure 8 shows comparison of polymer yield. It can be concluded that the reaction rate increases as the driving force increases. In both Figs. 7 and 8, it is shown that the reaction zone stops propagating after a certain time when $\Delta P_f$ is lower than 1500 Pa. In other words, the polymer in the central region cannot be decomposed, even if the temperature further increases, because the driving force is not strong enough to drive out the vapor generated in that region. Therefore, $\Delta P_f$ should be equal or higher than a critical value $\Delta P_{f,c}$ (in this example, $\Delta P_{f,c} = 1500$ Pa) to ensure polymer in the entire porous medium can be decomposed.

Third, the effect of filler particle size $d_1$ on the process is studied. Particle size of the filler has a strong influence on permeability of the porous medium, thus the vapor transport and reaction rate are influenced as well. Figure 9 shows the porosity comparison for $d_1 = 400$, 200, 100, and 40 $\mu$m. The initial porosities are $\varepsilon = 0.2$ and $\varepsilon_2 = 0.3$. It is shown that the reaction zone size increases as the $U_3O_8$ size increases. In addition, porosity gradient reduces as $U_3O_8$ size increases; therefore, uniformity of the product is enhanced. Figure 10 shows the comparison of polymer yield. It is shown that the reaction rate enhances as the $U_3O_8$ particle size increases, because the vapor can escape more easily as permeability increases.

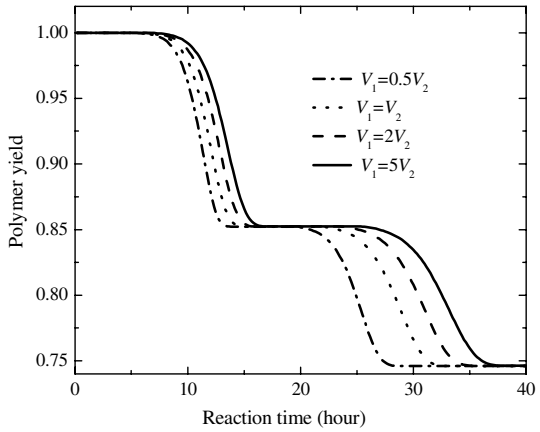


**Fig. 12 Comparison of polymer yields for different volume ratios $V_1/V_2$. Heat flux $q'' = 0.9$ W/m$^2$, $d_1 = 100$ $\mu$m, and initial porosity $\varepsilon = 0.2$.**

Finally, the influence of initial volume ratio of two different components is studied. The diameter of $U_3O_8$ is set as 100 $\mu$m; the initial porosity is $\varepsilon = 0.2$. Figure 11 shows the porosity comparison and Fig. 12 shows the comparison of polymer yield. It is shown that the porosity gradient decreases as the $U_3O_8$ volume increases, indicating that the product uniformity enhances. Moreover, the reaction rate is increased (Fig. 12) because the permeability of the porous medium increases as $U_3O_8$ volume increases. It can be concluded that the polymer pyrolysis rate and the product uniformity increases as $U_3O_8$ volume increases.

## VI. Conclusions

An advanced process model for polymer pyrolysis and uranium ceramic material processing is developed. The model is based on heat and mass transfer and reactions in a porous medium. The chemical reactions and their kinetics are established. The effect of sample geometry on the uniformity of product is studied. The results show that the reaction rate for polymer pyrolysis decreases and product uniformity reduces as the sample radius increases. The effect of different convection rates on the growth rate is shown. The reaction zone and rate increase, as well as the uniformity of product, as the driving force increases. There is a critical forced driving force, above which the polymer can decompose in the entire porous medium. The influence of the particle sizes on the reaction rate and product uniformity is presented. The results indicate that the polymer pyrolysis rate and product uniformity increase as the size of $U_3O_8$ increases. Finally, the effects of initial volume fraction of the filler $U_3O_8$ on the reaction rate and uniformity are studied. Those results clearly show that polymer pyrolysis rate and product uniformity increase when $U_3O_8$ volume increases.

## Acknowledgment

We would like to acknowledge the sponsorship from the U.S. Department of Energy Award (DE-FC07-05ID14673).

## References

[1] Hinoki, T., and Kohyama, A., "Current Status of SiC/SiC Composites for Nuclear Applications," *Annales de Chimie: Science des Matériaux*, Vol. 30, No. 6, 2005, pp. 659–671. doi:10.3166/acsm.30.659-671

[2] Berbon, M. Z., Dietrich, D. R., Marshall, D. B., and Hasselman, D. P. H., "Transverse Thermal Conductivity of Thin C/SiC Composites Fabricated by Slurry Infiltration and Pyrolysis: Ultrahigh-Temperature Ceramics," *Journal of the American Ceramic Society*, Vol. 84, No. 10, 2001, pp. 2229–2234.

[3] Alkan, Z., Kugeler, K., Kaulbarsch, R., and Manter, C., "Silicon Carbide Encapsulated Fuel Pellets for Light Water Reactors," *Progress in Nuclear Energy*, Vol. 38, Nos. 3–4, 2001, pp. 411–414. doi:10.1016/S0149-1970(00)00147-5

[4] Kotani, M., Inoue, T., Kohyama, A., Katoh, Y., and Okamura, K., "Effect of SiC Particle Dispersion on Microstructure and Mechanical Properties of Polymer-Derived SiC/SiC Composite," *Materials Science and Engineering A*, Vol. 357, No. 1, 2003, pp. 376–385. doi:10.1016/S0921-5093(03)00206-5

[5] Lee, Y. W., Lee, S. C., Kim, H. S., Joung, C. Y., and Degueldre, C., "Study on the Mechanical Properties and Thermal Conductivity of

Silicon Carbide-, Zirconia- and Magnesia Aluminate-Based Simulated Inert Matrix Nuclear Fuel Materials After Cyclic Thermal Shock," *Journal of Nuclear Materials*, Vol. 319, No. 1, 2003, pp. 15–23. doi:10.1016/S0022-3115(03)00128-4

[6] Lei, S., Shin, Y. C., and Incropera, F. P., "Experimental Investigation of Thermo-Mechanical Characteristics in Laser-Assisted Machining of Silicon Nitride Ceramics," *Journal of Manufacturing Science and Engineering*, Vol. 123, No. 4, 2001, pp. 639–646. doi:10.1115/1.1380382

[7] Greil, P., "Polymer Derived Engineering Ceramics," *Advanced Engineering Materials*, Vol. 2, No. 6, 2000, pp. 339–348. doi:10.1002/1527-2648(200006)2:6<339::AID-ADEM339>3.0.-CO;2-K

[8] Chan, W. C. R., Kelbon, M., and Krieger, B., "Modelling and Experimental Verification of Physical and Chemical Processes During Pyrolysis of a Large Biomass Particle," *Fuel*, Vol. 64, No. 11, 1985, pp. 1505–1513. doi:10.1016/0016-2361(85)90364-3

[9] Kotani, M., Katoh, Y., Kohyama, A., and Narisawa, M., "Fabrication and Oxidation-Resistance Property of Allylhydridopolycarbosilane-Derived SiC/SiC Composites," *Journal of the Ceramic Society of Japan*, Vol. 111, No. 1293, 2003, pp. 300–307. doi:10.2109/jcersj.111.300

[10] Staggs, J. E. J., "Modelling Thermal Degradation of Polymers Using Single-Step First-Order Kinetics," *Fire Safety Journal*, Vol. 32, No. 1, 1999, pp. 17–34. doi:10.1016/S0379-7112(98)00026-5

[11] Wang, X., Cai, D., and Zhang, H., "A Novel Method to Increase the Growth Rate in Sublimation Crystal Growth of Advanced Materials," *International Journal of Heat and Mass Transfer*, Vol. 50, Nos. 7–8, 2007, pp. 1221–1230. doi:10.1016/j.ijheatmasstransfer.2006.09.021

[12] Gann, R. G., Harris, R. H., Jr., Krasny, J. F., Levine, R. S., Mitler, H. E., and Ohlemiller, T. J., "The Effect of Cigarette Characteristics on the Ignition of Soft Furnishings," National Inst. of Standards and Technology Rept., 1988.

[13] Yang, W., Ponzio, A., Lucas, C., and Blasiak, W., "Performance Analysis of a Fixed-Bed Biomass Gasifier Using High-Temperature Air," *Fuel Processing Technology*, Vol. 87, No. 3, 2006, pp. 235–245. doi:10.1016/j.fuproc.2005.08.004

[14] Datta, A. K., and Zhang, J., "Porous Media Approach to Heat and Mass Transfer in Solid Foods," American Society of Agricultural Engineers Paper No. 99-3068, 1999.

[15] Interrante, L. V., Whitmarsh, C. W., Sherwood, W., Wu, H.-J., Lewis, R., and Maciel, G., "High yield polycarbosilaneprecursors to stoichiometric SiC," *Synthesis, Pyrolysis and Application in MRS Symposium Proceedings*, Vol. 346Materials Research Society, Warrendale, PA, 1994, pp. 593–603.

[16] Singh, A., Zunjarrao, S., and Singh, R. P., "Processing of Uranium Oxide and Silicon Carbide Based Fuel Using Polymer Infiltration and Pyrolysis," *Journal of Nuclear Materials*, Vol. 378, No. 3, Sept. 2008, pp. 238–243. doi:10.1016/j.jnucmat.2008.04.022

[17] Hurwitz, F. I., Kacik, T. A., Bu, X.-Y., Masnovi, J., Heimann, P., and Beyene, K., "Pyrolytic Conversion of Methyl- and Vinylsilane Polymers to Si-C Ceramics," *Journal of Materials Science*, Vol. 30, No. 12, 1995, pp. 3130–3136. doi:10.1007/BF01209227

[18] Cullity, B. D., "Elements of X-Ray Diffraction," Addison–Wesley, London, 1978.

[19] Kung, H., "A Mathematical Model of Wood Pyrolysis," *Combustion and Flame*, Vol. 18, No. 2, 1972, pp. 185–195. doi:10.1016/S0010-2180(72)80134-2

[20] Faghri, A., and Zhang, Y., *Transport Phenomena in Multiphase Systems*, Elsevier, New York, 2006.

[21] Moallemi, M. K., Zhang, H., and Kumar, S., "Numerical Modeling of Two-Dimensional Smoldering Process," *Combustion and Flame*, Vol. 95, Nos. 1–2, 1993, pp. 170–182. doi:10.1016/0010-2180(93)90059-C

[22] Zhang, H., Zheng, L., and Moallemi, M. K., "Transient Two-Dimensional Numerical Simulation of Laminar Flame Spread over a Porous Solid Fuel," *1995 National Heat Transfer Conference*, Vol. 304, American Society of Mechanical Engineers, Fairfield, NJ, Aug. 1995, pp. 53–62.

[23] Wang, X., Cai, D., and Zhang, H., "Increase of SiC Sublimation Growth Rate by Optimizing of Powder Packaging," *Journal of Crystal Growth*, Vol. 305, No. 1, 2007, pp. 122–132. doi:10.1016/j.jcrysgro.2007.03.022